On Crack Arrest in Ceramic / Metal Assemblies

by

Yann Charles and François Hild[*]

LMT-Cachan
ENS de Cachan / CNRS / Université Paris 6
61, avenue du Président Wilson
F-94235 Cachan Cedex, France

[*]To whom correspondence should be addressed
Fax: +33 1 47 40 22 40, Email: hild@lmt.ens-cachan.fr

On Crack Arrest in Ceramic / Metal Assemblies

by

Yann Charles and François Hild

Abstract

Brittle parts of ceramic/metal assemblies are subjected to a residual stress field generated by the fabrication. During that process, cracks are initiated and the key question is whether they propagate through the whole brittle part. The use of classical probabilistic fracture models applied to the ceramic (i.e., based on a weakest link hypothesis), allow one to conclude that cracks are likely to initiate after the manufacturing process. Consequently, a crack arrest model is proposed, based on a random toughness distribution. Applied to micro-hardness experiments, the statistical parameters are identified, and the predictive capacity of the model is analyzed. The model is then used to study the reliability of ceramic/metal assemblies during the fabrication stage.

Key Words

I.   Introduction

The use of components made of different materials (e.g., a ceramic/metal assembly) is interesting for industrial applications because of the presence of different physical properties. In a ceramic/metal assembly, the isolating properties even at high temperatures and the chemical inertia of the ceramic are used, whereas the metallic part provides its ductile behavior and its conducting capacities. These assemblies are used in different domains: medical (prosthesis, neuro-stimulator), electronic (connector), nuclear (recycling, storage), aeronautical (sensor). The ability of such components to sustain processing and in-service loadings is crucial.

The components studied herein are assembled at the melting temperature of the brazing joint (e.g., 780°C for an Ag-Cu eutectic). The dimensions of the different parts are controlled to be properly assembled at this temperature. Because of the coefficient of thermal expansion mismatch, thorn singularities arise when the elastic properties of the materials are identical (Bui and Taheri, 1989) and strong singularities when the elastic properties are different (Williams, 1959; Schmauder, 1989; Desmorat and Leckie, 1998). The residual stresses and these different singularities may generate the initiation and propagation of cracks in the brittle part of the component, eventually causing in-service failure.

Upon assembling the metallic and ceramic parts, crack initiation and propagation occurs because of the presence of processing defects (e. g., porosities or inclusions) induced by prior sintering of the ceramic. These defects are random in size and randomly distributed within the material. The initiation probability is therefore the probability of finding critical defects within the ceramic. A Weibull model (1939) can be used to evaluate the latter. Contrary to situations for which the initiation of a macro-crack leads to final failure of a structure (i.e., a weakest link hypothesis is made (Freudenthal, 1968)), there are situations for

which this hypothesis is not valid. For instance, multiple cracking may occur in impacted ceramics (Riou et al., 1998) or in fiber reinforced composites (Aveston and Kelly, 1973). In other cases, crack arrest may occur (e.g., ceramic/metal assemblies). Consequently, the weakest link framework has to be altered and the issue of crack arrest becomes the key element in assessing the reliability of the assembly after processing.

Crack arrest can be considered as finding one point where the crack propagation criterion is not met. In many cases this criterion is assumed to be deterministic (Griffith, 1921; Irwin, 1957). However there are experimental evidences to suggest that the critical value may be of statistical nature (Ponton and Rawlings, 1989b). Following the hypothesis proposed by Chudnowsky and Kunin (1987) or Jeulin (1994), it is assumed that the critical value is constant for each grain, but varies from one grain to another one. Consequently a probabilistic framework can be derived in which crack arrest is not deterministic but probabilistic.

Section II is devoted to the derivation of the probability of crack extension when the material toughness is randomly distributed. Section III addresses the general properties that can be deduced from the extension probability. Section IV deals with the identification of the toughness distribution for alumina (Al$_2$O$_3$) ceramics by using a micro-hardness experiment. Lastly, a practical situation is studied in Section V.

II.   Crack Arrest: a Probabilistic Approach

Since a Weibull model cannot be used to predict the ability of a brittle volume to experience crack arrest, the probabilistic conditions for crack arrest are analyzed. Following Chudnowsky and Kunin (1987), we assume that a brittle medium is composed of grains, with random toughness. The realization of this random variable is assumed to be grain-independent, and is characterized by a probability density function h_{K_c}. The toughness is

assumed to be constant for *each* grain (i.e., transgranular fracture) or *each* grain boundary (i.e., intergranular fracture). In all cases, we consider that the crack is submitted to an overall mode I loading.

II.1. A Simple Model for the Material Microstructure

In the following, we consider a 2D situation for which the crack path is aligned along the *x*-axis. It can be noted the results can be generalized to curved cracks. Each grain or grain boundary is a potential crack arrest site.

II.1.1. Transgranular Fracture

The most important feature of the grain distribution is its intersection with the considered crack path. As a first approximation, we assume that this intersection has a constant length $1/\lambda$ (Fig. 1). It follows that there are λ grains per unit length. The crack is submitted to a mode I condition along a given crack path, and its propagation stops when the following criterion is satisfied (Griffith, 1921; Irwin, 1957)

$$K_I(x) < K_c^k \tag{1}$$

where $K_I(x)$ is the stress intensity factor when the crack is at location *x*, and K_c^k the toughness of the kth grain. Besides, we consider that the failure of each grain of a given path is 'instantaneous,' and that the crack propagation is only transgranular. Let us consider a crack path composed by *N* grains. The probability that a crack propagates through all these grains is

$$P_N\left(\forall\, i \in \{1,...,N\}, K_I(x_k) > K_c^k\right), \tag{2}$$

where

$$K_I(x_k) = \min_{k^{th}\ grain} K_I(x). \tag{3}$$

Because of the grain-independent realization of the toughness, Eq. (2) becomes

$$P_N = \prod_{k=1}^{N} P\left(K_I(x_k) > K_c^k\right). \tag{4}$$

Equation (4) can be rewritten as

$$\ln(P_N) = \sum_{k=1}^{N} \ln\left[P\left(K_I(x_k) > K_c^k\right)\right]. \tag{5}$$

If the number of grains N becomes large, then a continuous formulation can be derived

$$\frac{1}{N}\sum_{k=1}^{N} \ln\left[P\left(K_I(x_k) > K_c^k\right)\right] \approx \frac{1}{b-a}\int_a^b \ln\left[P(K_I(x) > K_c)\right]dx, \tag{6}$$

where $\dfrac{b-a}{N}$ is the average grain length, i. e. $\dfrac{N}{b-a} = \lambda$. By knowing the probability density

function of toughness, one can determine the probability for a crack to propagate in mode I

from a length a to a length b on a given path

$$P(a,b) = \exp\left[\lambda\int_a^b \ln\left(P(K_I(x) > K_c)\right)dx\right], \tag{7}$$

with

$$P\left(K_I(x) > K_c\right) = \int_{K_c^{\min}}^{K_I(x)} h_{K_c}(k)dk, \tag{8}$$

where $K_c^{\min} \geq 0$ is the minimum value of the toughness of the considered material.

II.1.2. Intergranular Fracture

Crack propagation may also be intergranular. Let us assume that the boundary

between two grains is linear, and has a constant length $1/\lambda$. One random variable is the

orientation of the grain boundary θ $\left(\in \left]-\dfrac{\pi}{2},\dfrac{\pi}{2}\right[, \text{with respect of the overall propagation axis}\right)$.

It can be noted that the toughness and the elastic properties are also random variables. The

crack has a constant direction between two triple points, i.e., each point where three grains

intersect (Fig. 2). Crack propagation occurs when

$$G(x,\theta) > 2\Gamma \tag{9}$$

where $G(x,\theta)$ is the energy release rate of a kinked crack of length x and with a small extension of orientation θ, and Γ is the fracture energy of the grain boundary. By using weight functions (Bueckner, 1970; Rice, 1972), the energy release rate $G(x,\theta)$ under remote mode I conditions becomes

$$G(x,\theta) = \frac{K_I(x)^2}{E'} f(\theta), \tag{10}$$

with

$$f(\theta) = \left(\frac{3}{4}\cos\frac{\theta}{2} + \frac{1}{4}\cos\frac{3\theta}{2}\right)^2 + \left(\frac{1}{4}\sin\frac{\theta}{2} + \frac{1}{4}\sin\frac{3\theta}{2}\right)^2$$

$$E' = \begin{cases} E \text{ under plane strain condition} \\ \dfrac{E}{1-\nu^2} \text{ under plane stress condition} \end{cases} \tag{11}$$

where E is the Young's modulus and ν the Poisson's ratio of the uncracked material. The crack propagation criterion (9) can be written as

$$K_I(x) > \sqrt{\frac{2\Gamma E'}{f(\theta)}}. \tag{12}$$

We can conclude that when the crack propagates in an intergranular way in a random medium, we end up with an expression similar to that derived for transgranular fracture by introducing the random toughness $\widetilde{K}_c$ defined by

$$\widetilde{K}_c = \sqrt{\frac{2\Gamma E'}{f(\theta)}}. \tag{13}$$

Then, the probability for a crack propagating from a length a to a length b is

$$P(a,b) = \exp\left[\lambda \int_a^b \ln\left(P\left(K_I(x) > \widetilde{K}_c\right)\right)dx\right], \tag{14}$$

Equation (14) can be applied provided the correlation between two consecutive grain orientations is sufficiently small to influence the apparent toughness distribution $\widetilde{K}_c$ so that the realization of the random variable is still independent from grain boundary to grain boundary. Therefore, Eq. (7) can be used in the two situations.

II.2. Poisson Mosaic

Another statistical two-dimensional transgranular propagation model based on the random set theory (Matheron, 1975) has been established by Jeulin (1994). A Poisson tessellation of parameter λ defines the grain boundaries. The latter are made of Poisson lines in the plane for a two-dimensional medium. In particular, the probability that a segment of length l hits $N(l) = n$ grain boundaries is

$$P(N(l)=n)=\frac{(\lambda l)^n}{n!}e^{-\lambda l}, \tag{15}$$

where $N(l)$ is a random variable. The average number of grains per unit length is λ. It is also assumed that each grain has a constant toughness. By using a Griffith criterion on a crack of length x, one can compute the propagation probability to a length $x+dx$ for increasing stress intensity factors. The crack has a length x with a probability P(x). In a segment of length dx:

- there is one grain with a probability $P(N(dx)=0)\approx 1-\lambda dx$. Then the probability of propagating a crack to a length $x+dx$ is P(x), because of the increase of the stress intensity factor with x,

- there are two grains with a probability $P(N(dx)=1)\approx \lambda dx$. Then the probability for the crack to propagate to a length $x+dx$ is $P(K_I(x+dx)>K_c)P(x)$.

One can relate $P(x)$ and $P(x+dx)$ by

$$P(x+dx)=(1-\lambda dx)P(x)+\lambda dx P(x)P(K_I(x+dx)>K_c). \tag{16}$$

The following differential equation is obtained (Jeulin, 1994)

$$\frac{dP(x)}{dx} = -\lambda \big(1 - P(K_I(x) > K_c)\big) P(x). \tag{17}$$

By integrating Eq. (17), the propagation probability is expressed as

$$P(a,b) = \exp\left[-\lambda \int_a^b \big(1 - P(K_I(x) > K_c)\big) dx \right]. \tag{18}$$

We can note that Eq. (18) is very similar to Eqs. (7) and (13). For decreasing stress intensity factors, Eq. (16) becomes

$$P(x) = (1 - \lambda dx)P(x - dx) + \lambda dx P(x - dx)P(K_I(x) > K_c), \tag{19}$$

and the generated differential equation is the same as Eq. (17). Consequently, the propagation probability (18) is also true for decreasing stress intensity factors, and can be further generalized (Jeulin, 1994).

III. Probabilistic or DLH Effects

In brittle materials, when the weakest link hypothesis can be made, there are three key parameters to describe the failure probability:

- the defect distribution (that can be related to the Weibull parameter (Jayatilaka and Trustrum, 1977; Hild and Marquis 1992)),

- the volume of the structure (Freudenthal, 1968),

- the stress field heterogeneity (Davies, 1973; Hild and Marquis, 1992).

These three effects can be accounted for by the so-called effective volume (Davies, 1973).

Similarly, we can analyze three different effects in the present framework in which crack arrest occurs if one can find a strong grain for which the arrest criterion is satisfied. Consequently, there are three effects to be expected on the propagation probability:

- the effect of toughness distribution (D),

- the effect of the crack extension length (L) with respect to the grain size $1/\lambda$,

- the effect of stress heterogeneity (H).

To illustrate these effects, we consider a crack emanating from a hole (Fig. 3) for which closed-form solutions are available (Murakami, 1987).

III.1. D Effect: Effect of the Toughness Distribution

When the toughness distribution is different from one material to another one, the propagation probability is different. In particular, the upper tail (i.e., for high toughnesses) plays the most significant role since the arrest condition is related to finding grains with high toughnesses. In the following example, a Beta distribution is used. The probability density function is defined as

$$h_{K_c}(k) = \frac{\left(k - K_c^{\min}\right)^{\alpha-1}\left(K_c^{\max} - k\right)^{\beta-1}}{\left(K_c^{\max} - K_c^{\min}\right)^{\alpha+\beta-1} B(\alpha,\beta)}, \tag{20}$$

where B is the Euler (or Beta) function of the first kind (Spanier and Oldham, 1987). The average toughness $\overline{K}_c$ and the corresponding standard deviation $\overline{\overline{K}}_c$ are expressed as

$$\begin{cases} \overline{K}_c = \dfrac{\alpha}{\alpha+\beta} K_c^{\max} + \dfrac{\beta}{\alpha+\beta} K_c^{\min} \\ \overline{\overline{K}}_c^{2} = \dfrac{\alpha\beta}{(\alpha+\beta)^2(\alpha+\beta+1)}\left(K_c^{\max} - K_c^{\min}\right)^2 \end{cases} \tag{21}$$

Figure 4a shows two Beta distributions and Fig. 4b shows the probability of crack propagation when the remote stress field is tensile ($\sigma = 120$ MPa). When β is equal to 10, there are very few grains with a toughness of the order of $K_c^{\max} = 6\,MPa\sqrt{m}$, therefore, the propagation probability is high. When β is equal to 1.6, the crack propagation probability is lower since more grains are able to stop the crack (the average toughness is higher). When the crack path is under a tensile stress, the stress intensity factor is increasing with the crack

length. Consequently there exists a crack length x_0 such that $K_1(x_0) = K_c^{max}$. By using Eqs. (7) or (13), the extension probability from the length x_0 to any greater length becomes constant since no grain is able to stop the crack. As we can see in Fig. 4b, the length x_0 is less than the initial crack length.

III.2. L Effect: Effect of the Number of Traversed Grains

There is a combined effect of crack length and grains size (or number of grain per unit length). Therefore the product $\lambda(b-a)$, which represents the number of grains that are traversed by the crack extension $b-a$, is the key parameter to consider. Everything else being identical, when $\lambda(b-a)$ increases, the probability of crack extension decreases. This result is shown in Fig. 5 for two different grain sizes (50 μm and 67 μm). Let us consider two brittle media, whose grain size is $1/\lambda_1$ and $1/\lambda_2$, respectively. For a given crack path and a given mechanical configuration, the more grains are traversed, the higher the number of arrest sites (or grains) can be found. In particular, when $\lambda_1 < \lambda_2$, then $P_{\lambda_1}(a,b) > P_{\lambda_2}(a,b)$, since

$$P_\lambda(a,b) = \exp\left[-\lambda(b-a)\int_0^1 \ln\left(P\left(K_I((b-a)u+a) > K_c\right)\right)du \right] \qquad (22)$$

Conversely, when a unique medium is considered, for a given mechanical configuration, the higher the extension, the higher the number of traversed grains. The probability of finding an arrest site in the crack path (i.e., a grain with a high toughness) then increases, and the extension probability usually decreases (Fig. 5).

III.3. H Effect: Effect of Stress Heterogeneity

Last, there is an effect of the applied stress field: the more heterogeneous the stress field, the lower the propagation extension since arrest is more likely to occur. This effect can be recast as

$$P_{\sigma(x)}(a,b) = H^{\lambda(b-a)}P_{\sigma_{\max}}(a,b),$$ (23)

with

$$H = \exp\left[\frac{1}{b-a}\int_a^b \ln\left(\frac{P(K_I(x) > K_c)}{P(K_{\mathrm{I}max}(x) > K_c)}\right)dx\right],$$ (24)

where K_{Imax} is the stress intensity factor associated to a uniform tensile stress $\sigma_{\max}$ applied on the crack path, with $\sigma_{\max} = \max_{x \in [a,b]}\sigma(x)$. One can show, by using weight functions (Bueckner, 1970; Rice, 1972), that for any applied stress σ on a given crack path, with a maximum value $\sigma_{\max}$

$$K_\sigma(x) < K_{\sigma_{\max}}(x).$$ (25)

The factor H is referred to as stress heterogeneity factor and allows one to compare the effect of any stress field on crack propagation with a uniform (i.e., tensile) stress field. Figure 6 shows the stress heterogeneity effect when comparing a uniform stress field to a linear one for which the maximum value is reached at the hole (Point P of Fig. 3). The solid line of Fig. 6 is obtained with the remote tensile load and the dotted line is directly computed by using Eqs. (23) and (24) for a linearly decreasing remote stress.

IV.   Identification of the Toughness Distribution

One important part of present model is the evaluation of toughness distribution. In particular, we have to determine the toughness probability density function h_{K_c}. One of the ways to measure the toughness of a ceramic is to use Vickers micro-indentation (Palmqvist, 1957).

IV.1. Toughness Measurement

Even though the indentation principle (Fig. 7) is simple, there are many different ways to relate the indentation length a, the applied load F and the crack size c (Ponton and Rolling, 1989a, 1989b), that can be summarized by the following expression

$$K_c = \kappa \frac{F}{c^{3/2}} g(a, c, F), \tag{26}$$

where κ is a material-dependent parameter. Two main types of cracks can appear: radial cracks and so-called Palmqvist cracks (e.g., for WC-CO cermets): Fig. 8. For many authors, the function g is only hardness-dependent, therefore the toughness is written as

$$K_c = \kappa \frac{F}{c^{3/2}} g(a, \overline{H}), \text{ when } c/2a > 1, \tag{27}$$

where $\overline{H}$ is the hardness. A more recent study (Laval, 1995) shows that the toughness may be linearly related with $\dfrac{F}{c^{3/2}}$ and therefore $g = 1$. The parameter κ will be determined by using a comparison between the computed value of the average value $\overline{K_c}$ and the conventional K_{Ic} value (e.g., determined by using three point bend tests (Lemaitre and Piller, 1988)).

Indentation measurements are carried out on an alumina ceramic to identify the probability density function associated to the toughness distribution. It can be noted that the fracture process is intergranular for alumina. The applied force F is obtained by using the following masses M: 0.2 kg, 0.3 kg, 0.5 g and 1 kg applied for 15s.

IV.2. Identification of the Toughness Probability Density Function

On a polished surface, at least twenty indentations per applied mass have been performed. For low masses, (i.e., less than 0.3 kg), crack sizes are on the order of few grains, and the indentation process is not always able to create four measurable cracks. Furthermore,

some cracks, which have been stopped by a polishing-generated defect, are not considered. All the cracks whose length ratio $c/2a$ is less than unity are not accounted for because of necessary condition that allows the use of Eq. (27).

All the methods used to compute toughness are based on a homogeneous material. In the present case, the material is assumed to be composed of grains of random toughness. Therefore, even though the toughness values directly measured by using Eq. (27) cannot be considered, it gives a way of assessing the stress intensity factor of an indentation-generated crack. The toughness probability density function can then be determined by using the crack propagation model described in Section II.1. Since the number of traversed grains is small, an equivalent discrete expression is used instead of Eq. (7)

$$P(c) = \prod_{i=1}^{E(\lambda c)} P\left(\frac{\kappa F}{\left(\frac{i}{\lambda} \right)^{3/2}} > K_c \right) \left[(1-\delta) P\left(\frac{\kappa F}{c^{3/2}} > K_c \right) + \delta \right], \qquad (28)$$

where λc is the number of grains in the propagation length c, and δ is defined as

$$\delta = \begin{cases} 1 \text{ if } E(\lambda c) = \lambda c \\ 0 \text{ if } E(\lambda c) \neq \lambda c \end{cases},$$

where $E(x)$ is the floor function of the real x. By assuming that the toughness probability density function is a Beta function (Eq. (20)), Eq. (28) becomes

$$P\left(\frac{\kappa F \lambda^{3/2}}{i^{3/2}} > K_c \right) = \int_0^{\left(\frac{\kappa F \lambda^{3/2}}{i^{3/2} \Delta K} - \frac{K_c^{min}}{\Delta K} \right)} \left(\frac{t^{\alpha-1}(1-t)^{\beta-1}}{B(\alpha,\beta)} \right) dt \qquad (30)$$

with $\Delta K = K_c^{max} - K_c^{min}$. We can note that only four dimensionless parameters describe the propagation of indentation-generated cracks: α, β, $\dfrac{K_c^{min}}{\Delta K}$, the parameters of the Beta

distribution and $\dfrac{\kappa F \lambda^{3/2}}{\Delta K}$ a dimensionless parameter representative of the indentation test. An identification of these four parameters has been performed for alumina, based on the experimental results with a given indentation mass, i.e., the one with the most indentation-generated crack lengths. For the sake of simplicity, a least squares method is used (a maximum likelihood technique could have been used). The cumulative probability associated to a measured length is computed by using the following procedure: all the measured crack lengths are ordered in an increasing way, and

$$P\big(c < c_j\big) = \frac{j}{n+1}, \tag{31}$$

where c is the random crack length, c_j the jth experimental ordered value, and n the total number of experimental values.

The results obtained for M=0.3 kg have been considered for the identification (Table 1). Furthermore, when the material constants are identified, i.e., α, β, $K_c^{\min}$, the change of the indentation parameter $\dfrac{\kappa \lambda^{3/2}}{\Delta K}$, a priori hardness-dependent, can be determined for other values of M. Table 2 shows that this parameter is almost constant for alumina with an average value of 0.45 N^{-1}. Furthermore, we can see that for alumina, there is a predominance of low equivalent toughness values (i.e., low α, and high β). To determine the value of the indentation parameter κ, one has to know, for instance, the mean toughness of a ceramic. By using an independent experiment (Lemaitre and Piller, 1988), the average toughness K_{Ic} can be exhibited. It follows that the value of $K_c^{\max}$ can be related to α, β and K_{Ic} (when $K_c^{\min}=0$, see Eq. (21))

$$K_{Ic} = \frac{\alpha}{\alpha + \beta} K_c^{\max}. \tag{32}$$

For alumina, a value of $K_{Ic}=4.5$ MPa$\sqrt{\text{m}}$ can be found, so that $K_c^{\text{max}} = 19.2$ MPa$\sqrt{\text{m}}$. Figure 9a shows the toughness probability density function for alumina, and Fig. 9b a comparison between experimental results and predicted probabilities. Each solid line corresponds to an individual identification of the indentation parameter. The dashed lines are obtained when the indentation parameter $\dfrac{\kappa\lambda^{3/2}}{\Delta K}$ determined for M=0.3 kg is used for other masses. A good agreement is obtained that confirms the assumption of a constant indentation parameter $\dfrac{\kappa\lambda^{3/2}}{\Delta K}$ for the tested Al$_2$O$_3$ ceramic.

IV.3. Discussion: the Indentation Parameter

By using the proposed random propagation model, we can see that the experimental results of the indentation process for other masses can be predicted, once the different material properties are known. In particular, the basic hypothesis, that ceramics are composed of grains with random toughnesses is relevant. All of the derived considerations on the DLH effects can be observed. Furthermore, one can note the influence of the indentation mass on the experimental crack length: the higher the applied mass, the higher the extension probability. By using the expression of the stress intensity factor of indentation-generated cracks (Eq. (27)), the applied stress heterogeneity decreases with an increasing applied mass. The H effect is confirmed by experimental observations.

Once the toughness probability density function is determined, i.e., the values of α, β, K_c^{min} and K_c^{max}, the probabilistic propagation model (Eq. (7)) can be used to compute the extension probability of a real structure.

VI. Study of an Industrial Structure

The ability of a ceramic/metal assembly to survive the processing stage is conditioned by the resistance of its brittle part. The process induces a residual stress field, which may or may not stop initiated cracks.

V.1. Fabrication Process of the Studied Structure

The two main materials are a stainless steel (A304L) and a 97% purity alumina. The brazing joint is made of an Ag-Cu eutectic (Fig. 10). Since alumina is not a metallic material, classical brazing joints are unable to bond on its surface. First a metallisation of the alumina surface must be performed (Fell, 1994; Kara-Slimane, 1996). The aim of such a process is to create a continuous material from alumina to nickel, on which the brazing joint will bond (Fig. 11). Once this step is performed, the joining process can start. The different parts of the final structure (two stainless steel cylinders and an alumina one) are submitted to an increasing temperature from the room to the brazing joint melting temperature (i.e., 780°C). After the liquid brazing metal has penetrated between the different cylinders by capillarity, the external temperature is decreased to the room temperature thereby generating residual stresses.

V.2. Initiation in a Singular Stress Field

In the previous probabilistic treatment of crack propagation, the problem of crack initiation has not been analyzed. In the present case, singularities exist in the studied structure. They are responsible for the initiation of macro-cracks from initial flaws within the ceramic. A Weibull model will be used to asses the initiation probability even though a weakest link hypothesis is not made (i.e., initiation does not lead to final failure).

A strong singularity is generated either when there is a discontinuity in a structure geometry (crack tip, or angular point: Fig. 12) or when there is an elastic property mismatch. The stress field near these singularities is very high, thereby leading to crack initiation and propagation.

By using Weibull model, the initiation probability P_I near singularities can be computed

$$P_I = 1 - \exp\left[-\frac{1}{V_0} \int_\Omega \left(\frac{\langle \sigma_{eq}(x,y,z) \rangle}{S_0} \right)^m dxdydz \right]$$ (33)

where V_0 is an elementary volume, m the Weibull modulus (i.e., shape parameter), S_0 the scale parameter, $\sigma_{eq}(x,y,z)$ the maximum principal stress, $\langle . \rangle$ the Macauley brackets, and Ω the studied volume. The parameters m, S_0 and V_0 are material-dependent. Near a singular point, the stress field, in polar coordinates, has the following form

$$\underline{\underline{\sigma}}(r,\theta) = \frac{A}{r^p} \underline{\underline{\Sigma}}(\theta),$$ (34)

where $0 < p < 1$ is the singularity exponent, A a stress-dependent constant, and $\underline{\underline{\Sigma}}$ a correction function which is only dependent on the angle θ. The initiation probability in an area between a radius a and b (Fig. 12) is assessed by only considering the singular part of the stress field (Eq. (34)). The initiation probability P_I in the vicinity of a singular point only depends of the product pm:

- if $2 - pm \neq 0$

$$P_I = 1 - \exp\left[-\frac{\alpha_m \left(\Sigma_{eq}^{\max} \right)^m A^m}{V_0} \frac{b^{2-pm} - a^{2-pm}}{2 - pm} \right],$$ (35)

- if $2 - pm = 0$

$$P_I = 1 - \exp\left[-\frac{\alpha_m \left(\Sigma_{eq}^{\max}\right)^m A^m}{V_0} \ln\left(\frac{b}{a}\right) \right], \tag{36}$$

where $\Sigma_{eq}^{\max}$ represents the maximum positive principal value of the tensor $\underline{\underline{\Sigma}}$, and α_m is a

constant generated by the integration of Eq. (33)

$$\alpha_m = \frac{1}{S_0^{\ m}} \int_\theta \left(\frac{\left\langle \Sigma_{eq}(\theta) \right\rangle}{\Sigma_{eq}^{\max}} \right)^m d\theta \,. \tag{37}$$

When a vanishes, the initiation probability computed by Eqs. (35) and (36) becomes the

initiation probability induced by a singular point, and then, for any A, V_0, S_o and $\underline{\underline{S}}$, if $pm \geq 2$,

then $P_I\left(\Sigma_{eq}^{\max} = 0^+\right) = 1$, and if $pm < 2$, then $P_I\left(\Sigma_{eq}^{\max} = 0^+\right) < 1$. For a given singular point, only

the Weibull modulus m will determine the ability of a structure to resist to a singular stress.

This modulus being material-dependent, the knowledge of the singularity exponent will

determine the initiation conditions (Lei et al., 1998).

It can be noted that these results can be further generalized by accounting for

singularities arising in bi-materials. It is still the product of the singularity exponent, or its real

part for an oscillating solution (Suo, 1990), by the Weibull modulus that has to be compared

to 2 (Charles, 2002).

V.3. Crack Extension

The fabrication process is simulated by using the FE code Castem2000 (Laborderie

and Jeanvoine, 1995). A viscoplastic model (Lemaitre et Chaboche, 1988) is used for the

stainless steel and an elastic perfectly viscoplastic model for the brazing joint (Lovato, 1995).

The ceramic is assumed to be perfectly elastic (Appendix). In the thermomechanical

computation, the temperature field is assumed to be uniform since the maximum temperature

rate (i.e., $-0.4°C.s^{-1}$) is small compared with the outer radius (i.e., 13.7 mm). Figure 13 shows

a map of equivalent stresses (the von Mises stress in stainless steel and the brazing joint, and the maximum principal stress in alumina). One can note the potential initiation and propagation sites. The finite elements (i.e., so-called Barsoum (1976) elements) near these singular points shown in Fig. 13 enable one to evaluate the singularity exponents. By using the map of equivalent stresses and the Weibull model (Eq. (33)), a map of initiation probabilities in the ceramic part at the end of the cooling process can be obtained (Fig. 14). The Weibull parameters used to perform this computation are $V_0 = 10^{-9}$ m^3, $S_0 = 200$ MPa, and $m = 10$ (Fett and Munz, 1994). By using Eqs. (35) and (36) and the results of Section V.2., one can conclude that all the singularity exponents p are such that $pm \geq 2$, i.e., $P_I\left(\Sigma_{eq}^{max} = 0^+\right) = 1$. Consequently four cracks are likely to initiate from flaws located near these singularities.

By using the map of equivalent stresses (Fig. 13), some crack paths can be determined: all of them are initiated in the vicinity of a singular point, and they are always perpendicular to the maximum principal directions (Fig. 15a). At the singular point no. 1, at least two directions of propagation may occur. Furthermore, some singularity exponents (point no. 3 and no. 5) have been computed at $t = 0^+$ and at the end of the cooling process (Table 3). Because of the non-linear behavior of the brazing joint and the stainless steel, these exponents are higher at the beginning of the cooling process than at the end.

On few determined crack paths, i.e., the ones that might be the more dangerous for the structure life, the applied stresses have been extracted from the FE computation of the cooling process, and by using weight functions (Bueckner, 1970; Rice, 1972) and Eq. (7), the propagation probabilities of all these cracks are computed (Fig. 15b). The toughness density probability function corresponds to the one identified in Section IV (Table 1). None of the five studied cracks can propagate through the whole alumina structure. But the propagation probability can be initially high for a small initiation crack length a (Eq. (7)). Then, some

cracks are existing in ceramic/metal assemblies but they are arrested near compressive or low tensile zones. This has been confirmed by the manufacturer of the studied assemblies (Duval, 2000).

VI. Conclusions

This study on ceramic/metal assemblies allows us to exhibit a random crack propagation model, based on a microstructural hypothesis, i.e., a random toughness of each grain or grain boundary of a brittle medium, that can explain their reliability after the manufacturing process. The DLH effects, derived from the model, account for the toughness distribution, propagation length relative to grain size and the stress field heterogeneity on the crack extension probability. This model has been applied to micro-hardness experiments and after an identification of the different material parameters, i.e., the toughness probability density function and the indentation parameter for a given load, it leads to a good predictions of the measured indentation-generated crack length for other load levels for alumina. The model is then applied to a real structure to determine the influence of the manufacturing process on crack initiation and propagation in the brittle part.

The use of such a probabilistic approach allows for the computation of the crack propagation probability for each identified path. A second step of the study would be the consideration of a fatigue crack propagation model. The propagation of the different cracks in the alumina part with an increasing time has to be computed, and a lifing procedure of such ceramic/metal assemblies can then be devised. This work is still in progress.

VII. Acknowledgements

VIII. References

Aveston J. and Kelly A., 1973. Theory of Multiple Fracture in Fibrous Composites, *J. Mat. Sci.*, **8**, 352-362.

Barsoum S. R., 1976. On the Use of Isoparametric Finite Elements in Linear Fracture Mechanics, *Int. J. Numer. Meth. Eng.*, **10**, 25-37.

Bueckner H. F., 1970. A Novel Principle for the Computation of Stress Intensity Factors, *Zeitschrift für Angewandte Mathematik und Mechanik*, **50**, 9, 529-546.

Bui H. D. and Taheri S., 1989. La singularité épine dans les bi-matériaux en thermo-élasticité, *C. R. Acad. Sci. Paris*, **309**, Série II, 1527-1533.

Charles Y., 2002. *Identification d'un mode de vieillissement dans un assemblage céramique-métal*, PhD dissertation, Ecole Normale Supérieure de Cachan (France), in French.

Chudnowsky A. and Kunin B., 1987. A Probabilistic Model of Brittle Crack Formation, *J. Appl. Phys.*, **62** 10, 4124.

Davis D. G. S., 1973. The Statistical Approach to Engineering Design in Ceramics, *Proc. Brit. Ceram. Soc.*, **22**, 429-452.

Desmorat R. and Leckie F. A., 1998. Singularities in Bi-Materials: Parametric Study of an Isotropic/Anisotropic Joint, *Eur. J. Mech. A/Solids*, **17,** 1, 33-52.

Duval J., 2000. Personal Communication.

Fell P., 1994. Active Metal Braze Alloys for Joining Metals to Ceramics, *Advances in Joining Technology 26 Oct.*, The British Association for Brazing and Soldering.

Fett T. and Munz D., 1994. Lifetime Prediction for Ceramic Materials under Constant and Cyclic Load, Life Prediction Methodologies and Data for ceramic Materials, ASTM STP 1201, Brinkman C. R. and Duffy S. F. Edts., *Am. Soc. Test. Mat.*, Philadelphia (USA), 161-174.

Freudenthal A. M., 1968. Statistical Approach to Brittle Fracture, in: Liebowitz H. (Ed.), *Fracture*, Academic Press, New York (USA), **2**, 591-619.

Griffith A. A., 1921. The Phenomenon of Rupture and Flow in Solids, *Trans. Roy. Soc. London*, A **221**, 163-198.

Hild F. and Marquis D., 1992. A Statistical Approach to the Rupture of Brittle Materials, *Eur. J. Mech. A/Solids*, **11**, 6, 753-765.

Irwin G. R., 1957. Analysis of the Stresses and Strains near the End of a Crack Traversing a Plate, *J. Appl. Mech.*, **24**, 361-364.

Jayatilaka A. de S. and Trustrum K., 1977. Statistical Approach to Brittle Fracture, *J. Mat. Sci.*, **12**, 1426-1430

Jeulin D., 1994. Fracture Statistics Models and Crack Propagation in Random Media, *Appl. Mech. Rev.*, **47**, 1, Part. 2, 141-150.

Kara-Slimane A., 1996. *Assemblages métal-céramiques (oxydes, nitrures) par métallisation brasage; influence des interactions chimiques dans les zones interstitielles*, PhD dissertation, Ecole Centrale de Lyon (France), in French.

Laborderie C. and Jeanvoine E., 1995. Beginning with Castem2000, *CEA Rapport no. 94/356.* LAMS. http://semt2.smts.cea.fr:8001/~bris/DOC/presentation_castem_English.html.

Laval P., 1995. *Etude théorique et expérimentale de l'indentation des matériaux élastoplatiques homogènes ou revêtus*, PhD dissertation, Ecole Nationale Supérieure des Mines de Paris (France), in French.

Lei Y., O'Dowd N. P., Busso E. P. and Webster G. A., 1998. Weibull Stress Solutions for 2-D Cracks in Elastic and Elastic-Plastic Materials, *Int. J. Fract.*, **89**, 245-268.

Lemaitre J. and Chaboche J.-L., 1988. *Mécanique des matériaux solides*, Dunod, Paris (France). English translation: Lemaitre J. and Chaboche J.-L., 1990. *Mechanics of Solid Materials*, Cambridge University Press, Cambridge (UK).

Lemaitre P. and Piller R., 1988. Comparison of the Fracture Toughness of Alumina by Three Different Methods, *J. Mat. Sci. Lett.*, **7**, 772-774.

Lovato G., 1995. *Rhéologie des joints brasés: étude expérimentale et détermination par méthode inverse,* PhD dissertation, Ecole Nationale Supérieure des Mines de Paris (France), in French.

Matheron G., 1975. *Random Set and Integral Geometry,* J. Wiley and Sons, New York (USA).

Murakami Y., 1987. *Stress Intensity Factors Handbook*, Pergamon Press, Oxford (UK).

Palmqvist S.,1957. Jernkontorets Ann., **141**, 5, 300-307. See also: K. Niihara, R. Morena and D.P.H. Hasselman, 1982. Evaluation of K_{1c} of brittle solids by the indentation method with low crack-to-indent ratios, *J. Mat. Science Lett.*, **1**, 13-16.

Ponton C. B. and Rawling R. D., 1989a. Vickers Indentation Fracture Toughness Test- Part1 − Review of Literature and Formulation of Standardised Indentation Toughness Equation, *Mat. Sci. Tech.*, **5**, 865-872.

Ponton C. B. and Rawling R. D., 1989b. Vickers Indentation Fracture Toughness Test- Part2 – Application and Critical Evaluation of Standardised Indentation Toughness Equation, *Mat. Sci. Tech.*, **5**, 961-976.

Rice J. R., 1972. Some Remarks on Elastic Crack Tip Stress Fields, *Int. J. Solids Struct.*, **8**, 751-758.

Riou P., Denoual C. and Cottenot C. E., 1998. Visualisation of the Damage Evolution in Impacted Silicon Carbide Ceramic, *Int. J. Impact Eng.*, **21**, 225-235.

Schmauder S., 1989. Influence of Elastic Anisotropy on the Edge Problem, *Metal-Ceramic Interfaces*, **4**, 413-419.

Spanier J. and Oldham K. B., 1987. The Incomplete Beta Function B(ν,μ,x), *Atlas of functions*, Hemisphere Ed., Washington DC (USA), chap. 58, 573-580.

Suo Z., 1990. Singularities, Interfaces and Cracks in Dissimilar Media, *Proc. Roy. Soc. London,* A **427**, 331-358.

Weibull W., 1939. A Statistical Theory of the Strength of Materials, *Proc. Roy. Swed. Ins. Eng. Research.* **151**, 1-45

Williams M. L., 1959. The Stress Around a Fault or Crack in Dissimilar Media, *Bull. Seismol. Soc. Am.*, **49**, 199-204

Appendix

The constitutive equations modeling the thermomechanical behavior of A304L stainless steel and the brazing joint (i.e., Ag-Cu eutectic) are based on the following viscoplastic model (Lemaitre and Chaboche, 1985). A small strain partition is assumed

$$\underline{\underline{\varepsilon}} = \underline{\underline{\varepsilon}}^e + \underline{\underline{\varepsilon}}^p + \underline{\underline{\varepsilon}}^{th} \tag{A1}$$

where $\underline{\underline{\varepsilon}}$ denotes the infinitesimal strain tensor, $\underline{\underline{\varepsilon}}^p$ the plastic strain tensor, $\underline{\underline{\varepsilon}}^{th}$ the thermal strain tensor, and $\underline{\underline{\varepsilon}}^e$ the elastic strain tensor related to the Cauchy stress tensor $\underline{\underline{\sigma}}$ by

$$\underline{\underline{\varepsilon}}^e = \frac{1+\nu}{E}\underline{\underline{\sigma}} - \frac{\nu}{E}\underline{\underline{\sigma}} : \underline{\underline{1}} \tag{A2}$$

and

$$\underline{\underline{\varepsilon}}^{th} = \alpha_{th}(T - T_{ref}) : \underline{\underline{1}} \tag{A3}$$

where E and ν denote the Young's modulus and Poisson's ratio, respectively, α_{th} the coefficient of thermal expansion, ':' the contraction with respect to two indices, $\underline{\underline{1}}$ the unit tensor, T the current temperature and T_{ref} a reference temperature. The viscoplastic model is based on non-linear kinematic and isotropic hardenings within the framework of the J_2 flow rule so that the strain rate tensor $\underline{\underline{\dot{\varepsilon}}}^p$ can be written as

$$\underline{\underline{\dot{\varepsilon}}}^p = \frac{3}{2} \frac{\left(\underline{\underline{S}} - \underline{\underline{X}}\right)}{J_2\left(\underline{\underline{S}} - \underline{\underline{X}}\right)} \dot{p}_p$$

$$\text{with } \dot{p}_p = \left(\frac{\langle f \rangle}{K_n}\right)^n \text{ and } f = J_2\left(\underline{\underline{S}} - \underline{\underline{X}}\right) - R - \sigma_y \tag{A4}$$

where $\dot{p}_p$ is the cumulative plastic strain rate, $\underline{\underline{S}}$ is the deviatoric part of the stress tensor, $\underline{\underline{X}}$ the kinematic hardening variable and R the isotropic hardening variable, J_2 the second

invariant of any considered tensor, $\langle . \rangle$ the Macauley brackets, K_n and n material parameters, and σ_y the yield stress. The kinetic laws for the hardening variables are given by

$$
\begin{aligned}
\dot{\underline{\underline{X}}} &= \frac{2}{3}C\dot{\underline{\underline{\varepsilon}}}^p - \gamma\underline{\underline{X}}\dot{p}_p \\
\dot{R} &= b_R(Q-R)\dot{p}_p
\end{aligned}
\tag{A5}
$$

where C, γ, b_R, Q are material parameters. Table A1 summarizes the parameters used in the computation to model the viscoplastic behavior of A304L. For the brazing joint, an elastic and purely viscoplastic model is chosen. The plastic strain rate tensor is then expressed as

$$
\dot{\underline{\underline{\varepsilon}}}^p = \frac{3}{2}\left(\frac{\langle J_2(\underline{\underline{S}})-\sigma_y\rangle}{K_n}\right)^n \frac{\underline{\underline{S}}}{J_2(\underline{\underline{S}})}.
\tag{A6}
$$

The corresponding material parameters are reported in Table A2. Table 3 gives the parameters used to model an alumina ceramic.

Table A1. Parameters for A304L stainless steel.
A linear interpolation is used for intermediate temperatures.

T (°C)	E (GPa)	ν	α_{th} (C^{-1})	σ_y (MPa)	Q (MPa)	b_R	C (MPa)	γ	K_n (MPa)	n
20	196	0.29	15.7 x 10^{-6}	250	60	8	162	2800	151	24
600	137	0.29	19.4 x 10^{-6}	130	80	10	24	300	150	12

Table A2. Parameters for Ag-Cu eutectic (after (Lovato, 1995)).
A linear interpolation is used for intermediate temperatures.

T (°C)	E (GPa)	ν	α_{th} (C^{-1})	σ_y (MPa)	K_n (MPa)	n
20	95	0.37	18.2 x 10^{-6}	247	85	10.1
100	95	0.37	18.2 x 10^{-6}	183	79	9.3
200	95	0.37	18.2 x 10^{-6}	87	38	7.2
300	95	0.37	18.2 x 10^{-6}	40	31	6.9
400	95	0.37	18.2 x 10^{-6}	27	13	4.9
500	95	0.37	18.2 x 10^{-6}	13	7	3.2
600	95	0.37	18.2 x 10^{-6}	6	6	1.2
700	95	0.37	18.2 x 10^{-6}	2	6	1.2

Table A3. Parameters for an alumina ceramic.

E (GPa)	ν	α_{th} (C^{-1})	S_0 (MPa)	V_0 (m^3)	m
330	0.26	7.9 x 10^{-6}	200	10^{-9}	10

Figure Caption

Figure 1: Crack path for transgranular propagation.

Figure 2: Pattern of the microstructure boundary for intergranular propagation. under an overall mode I loading

Figure 3: Geometry used for numerical simulations (a = 0.1 mm, R = 5 mm). Two different remote stress fields are considered. A uniform stress along the normal to the crack face and a linearly decreasing stress (−20 MPa/mm) whose maximum value is identical to that of the uniform field when $a = 0$.

Figure 4:

-a- Two different toughness distributions with a constant standard deviation $\left(\overline{\overline{K}}_c = 0.46\,\text{MPa}\sqrt{\text{m}}\right)$ and different averages $\left(2.7\,\text{MPa}\sqrt{\text{m}} \text{ and } 5\,\text{MPa}\sqrt{\text{m}}, \text{respectively}\right)$

-b- Crack extension probabilities for the two distributions ($\sigma = 120$ MPa, $K_c^{\min} = 0\,\text{MPa}\sqrt{\text{m}}$,

$K_c^{\max} = 6\,\text{MPa}\sqrt{\text{m}}$, $\lambda = 10^5\,\text{m}^{-1}$, and a = 10^{-4} m).

Figure 5: Crack extension probability for different values of λ ($\sigma = 80$ MPa, $K_c^{\min} = 0$ $\text{MPa}\sqrt{\text{m}}$, $K_c^{\max} = 6\,\text{MPa}\sqrt{\text{m}}$, $\alpha = 8$, $\beta = 10$, and a = 10^{-4} m)

Figure 6: Influence of the applied stress field on the crack propagation probability ($\sigma_{max} = 120$ MPa, $K_c^{min} = 0$ MPa$\sqrt{m}$, $K_c^{max} = 6$ MPa$\sqrt{m}$, $\alpha = 8$, $\beta = 10$, $\lambda = 10^5$ m^{-1}, and a $= 10^{-4}$ m)

Figure 7: Toughness measurements based on micro-indentation experiments

Figure 8: Different crack systems generated by indentation.

Figure 9:

-a- Identified toughness distribution for alumina.

-b- Extension probability versus crack length for different applied masses on alumina.

Figure 10: Studied ceramic/metal assembly.

Figure 11: Interface generated by the metallisation process.

Figure 12: Geometry near a singular point.

Figure 13: Equivalent stresses in the structure (von Mises stresses in the ductile parts and maximum principal stress in the ceramic) at the end of the processing stage.

Figure 14: Map of the initiation probability in the alumina part.

Figure 15:

-a- Possible crack paths in the alumina part (a=2.2 x 10^{-4} m)

-b- Propagation probabilities for the different crack paths.

Table Caption

Table 1: Toughness parameters for a 97% alumina ceramic.

Table 2: Indentation parameter $\dfrac{\kappa\lambda^{3/2}}{\Delta K}$ for different applied masses (average value: 0.45 N^{-1}).

Table 3: Singularity exponent at different singularity points at the beginning and the end of the fabrication process

Table 1: Charles and Hild

λ (m^{-1})	α	β	$K_c^{\max}$ $\left(\text{MPa}\sqrt{\text{m}}\right)$	$K_c^{\min}$ $\left(\text{MPa}\sqrt{\text{m}}\right)$	M (kg)	$\dfrac{\kappa\lambda^{3/2}}{\Delta K}$ (N^{-1})
5.10^5	2.8	9.1	19.2	0	0.3	0.45

Table 2: Charles and Hild

Mass M (kg)	0.2	0.3	0.5	1
$\dfrac{\kappa\lambda^{3/2}}{\Delta K}$ (N^{-1})	0.52	0.45	0.44	0.45

Table 3: Charles and Hild

Singularity	Singularity exponent at the beginning of the cooling process	Singularity exponent at the end of the cooling process
no. 3	0.41	0.22
no. 5	0.70	0.19

Figure Caption

Figure 1: Crack path for transgranular propagation

Figure 2: Pattern of the microstructure boundary for an intergranular propagation

Figure 3: Geometry used for numerical simulations

Figure 4a: Two different toughness distributions, with a constant standard deviation $\left(\overline{\overline{K}}_c = 0.46 \text{ MPa}\sqrt{m}\right)$ and different averages $\left(2.7 \text{ MPa} \sqrt{m} \text{ and } 5 \text{ MPa} \sqrt{m}, \text{ respectively }\right)$

Figure 4b: Crack extension probabilities for two different Beta distributions with different averages and constant standard deviation (σ=120 MPa, K_c^{min}=0 MPa$\sqrt{m}$, K_c^{max}=6 MPa$\sqrt{m}$, λ=10^5 m^{-1}, and a=10^{-4} m)

Figure 5: Crack extension probability for different values of λ (σ=80 MPa, K_c^{min}=0 MPa$\sqrt{m}$, K_c^{max}=6 MPa$\sqrt{m}$, α=8, β=10, and a=10^{-4} m)

Figure 6: Influence of the applied stress field on the crack propagation probability (σ_{max}=120 MPa, K_c^{min}=0 MPa$\sqrt{m}$, K_c^{max}=6 MPa$\sqrt{m}$, α=8, β=10, λ=10^5 m^{-1}, and a=10^{-4} m)

Figure 7: Toughness determination by micro-indentation measurement

Figure 8: Different crack systems generated by indentation

Figure 9a: Identified toughness distribution for alumina

Figure 9b: Extension probability versus crack length for different applied masses

Figure 10: Studied ceramic/metal assembly

Figure 11: Interface generated by the metallisation process

Figure 12a: Geometry near a singular point

Figure 12b: Half-infinite assembled materials

Figure 13: Equivalent stresses in the structure (von Mises stresses in the ductile part and maximum principal stress in the ceramic) at the end of the processing stage

Figure 14: Numerical computation of the initiation probability in the alumina part

Figure 15a: Possible crack paths in the alumina part (a=2.210^{-4} m)

Figure 15b: Propagation probabilities for the different crack paths
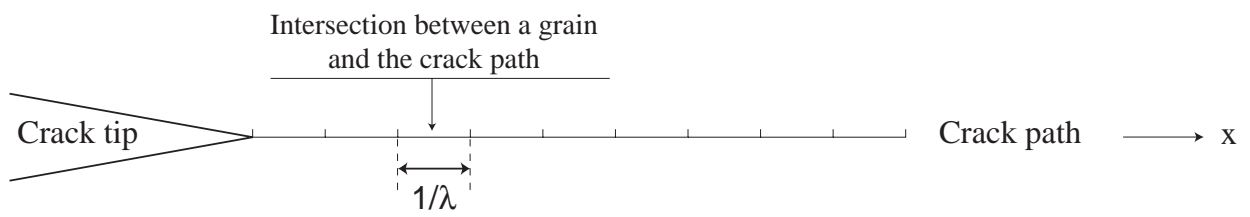
Figure 1: Charles and Hild

Figure 2: Charles and Hild
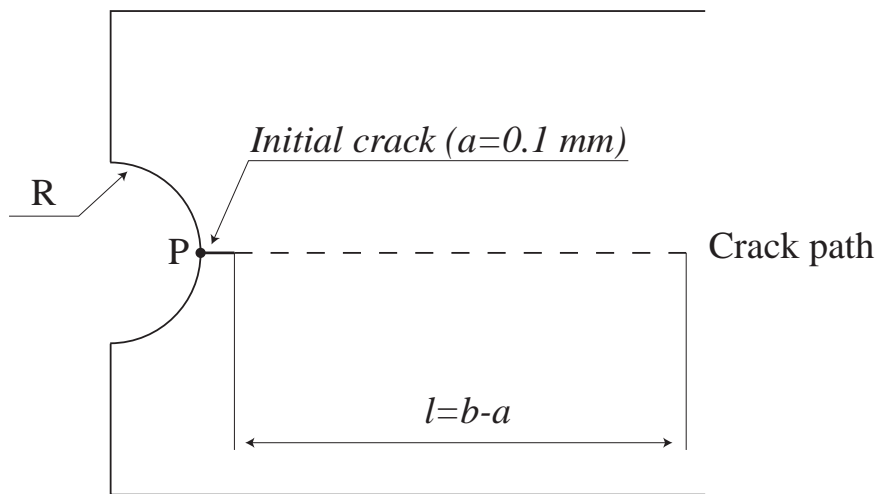
Figure 3: Charles and Hild
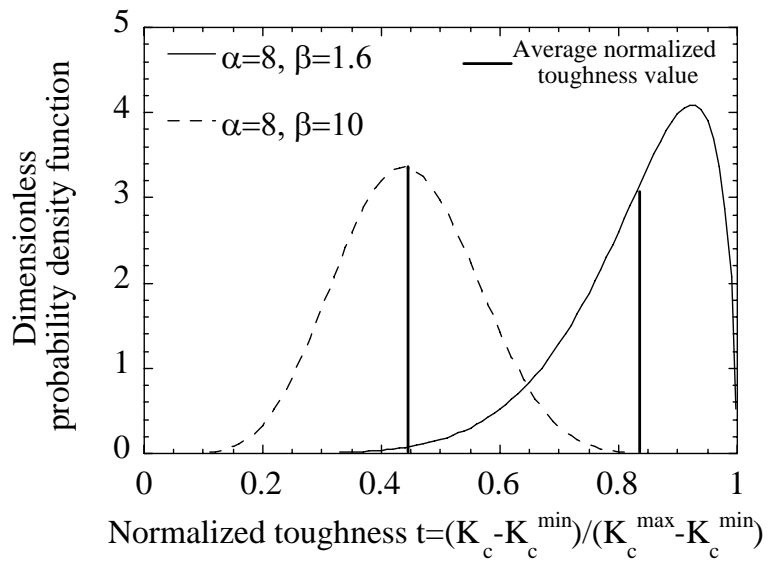
Figure 4a: Charles and Hild
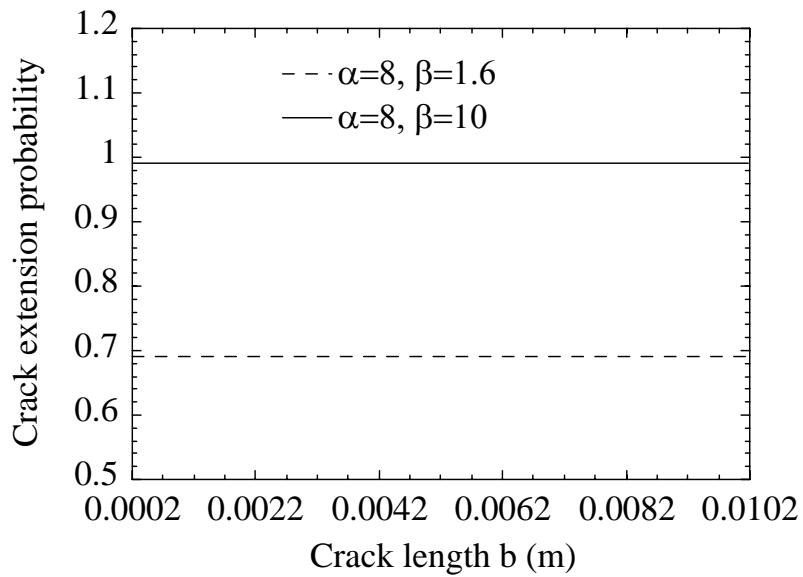
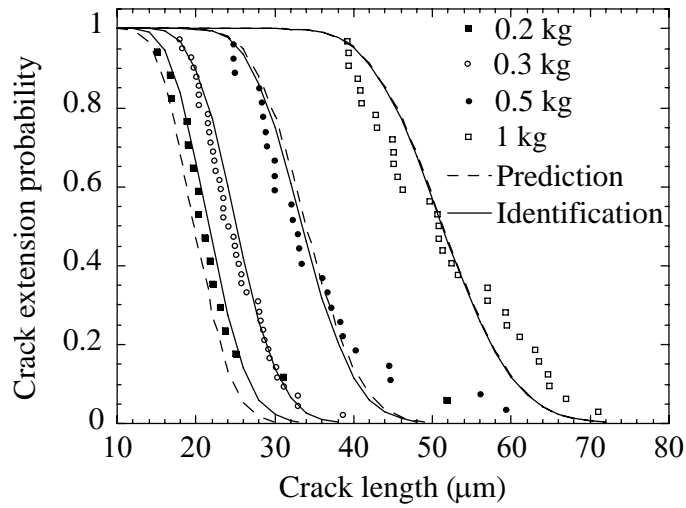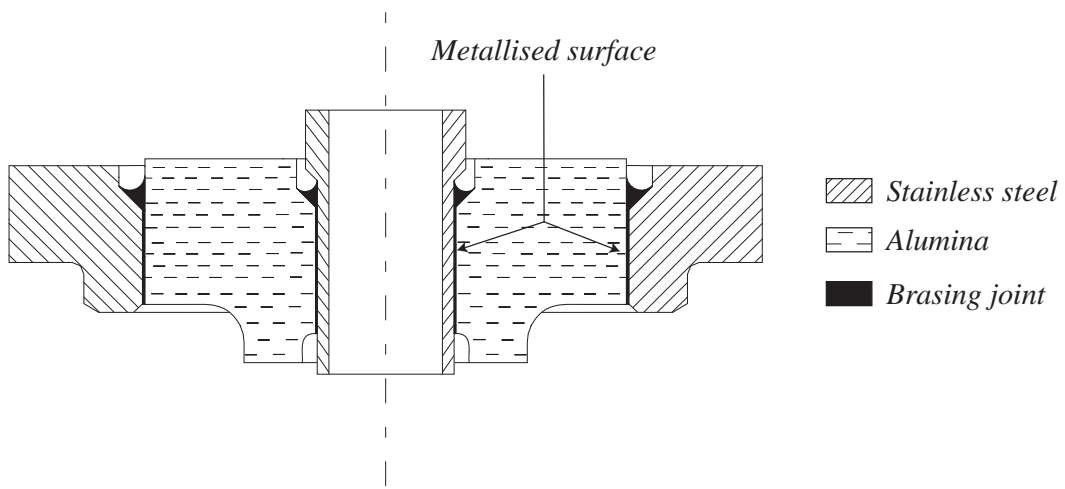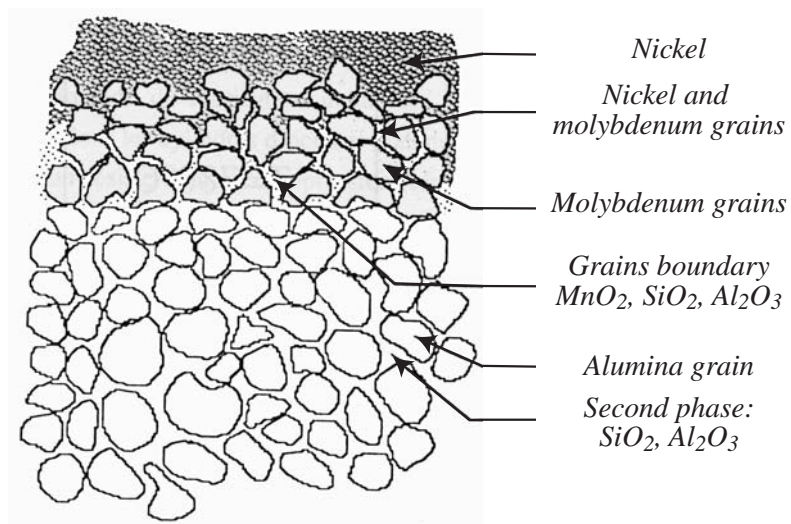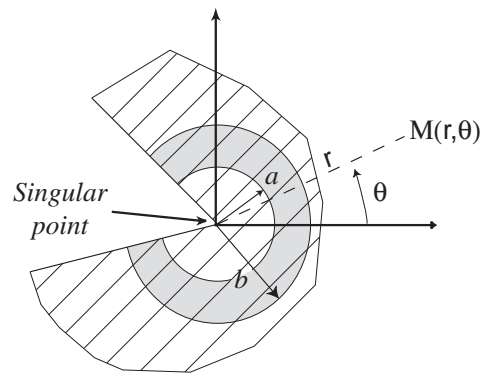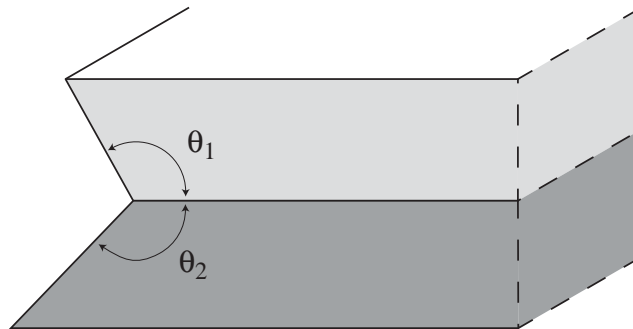
Figure 4b: Charles and Hild
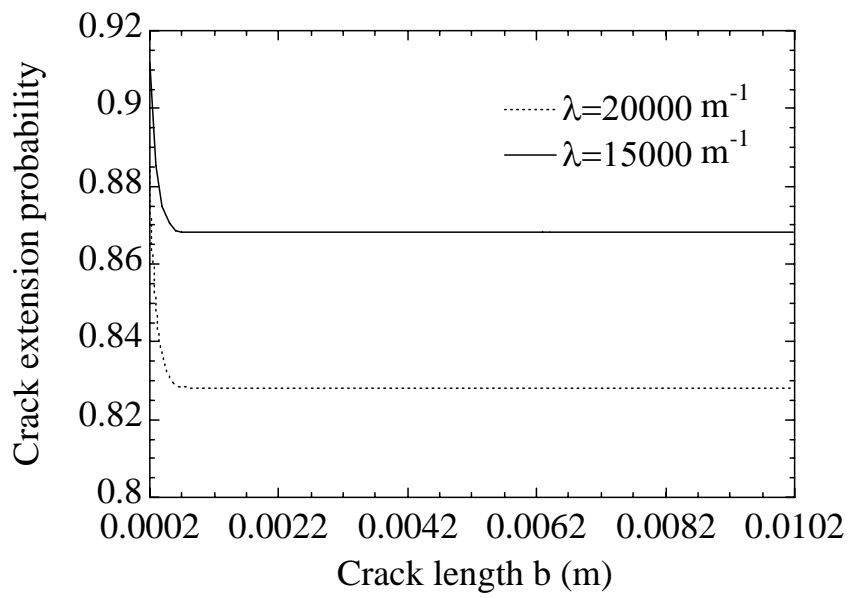
Figure 5: Charles and Hild
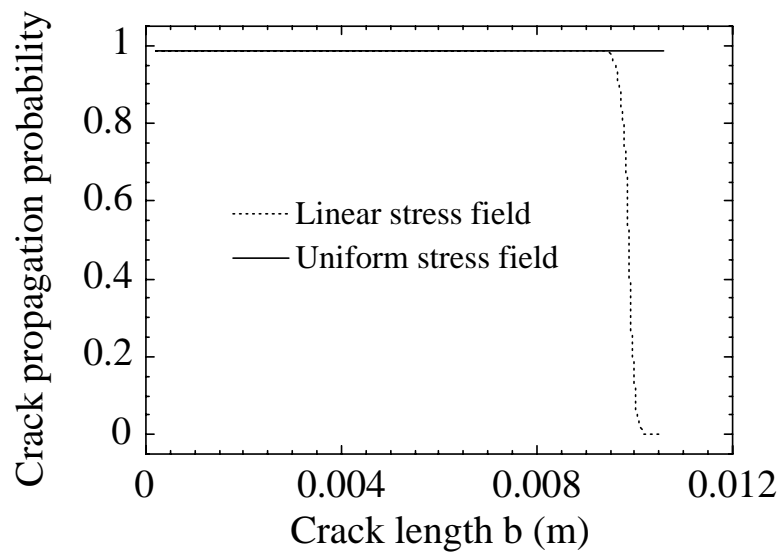
Figure 6: Charles and Hild
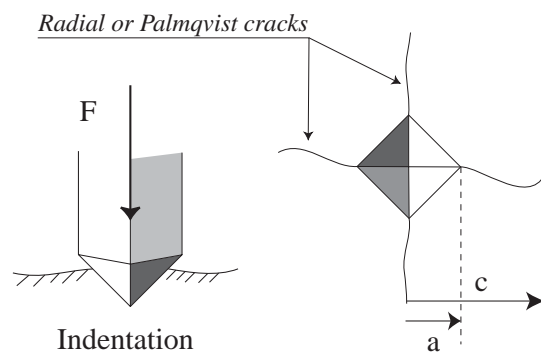
Figure 7: Charles and Hild

Radial crack system   *Palmqvist crack system*
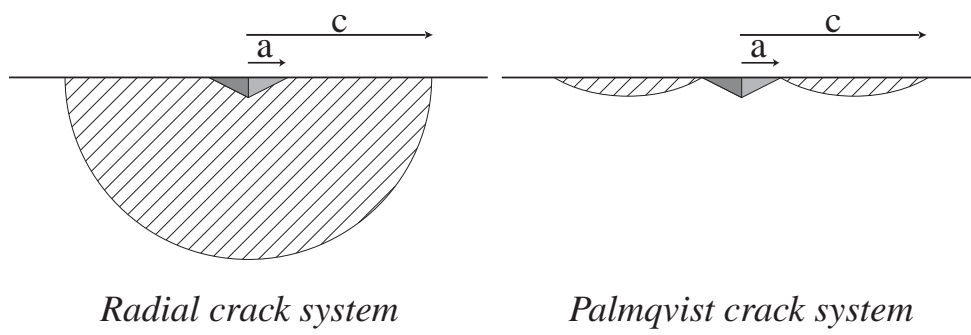
Figure 8: Charles and Hild
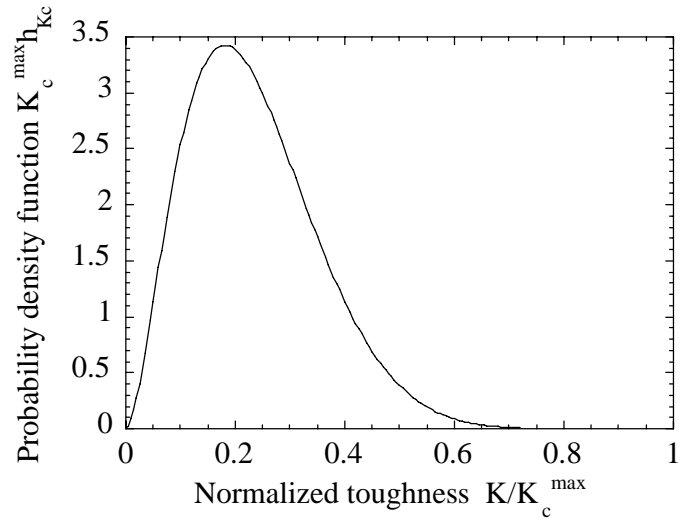
Figure 9a: Charles and Hild

Figure 9b: Charles and Hild

Metallised surface

Stainless steel

Alumina

Brasing joint

Figure 10: Charles and Hild

Figure labels:
- Nickel
- Nickel and molybdenum grains
- Molybdenum grains
- Grains boundary MnO_2, SiO_2, Al_2O_3
- Alumina grain
- Second phase: SiO_2, Al_2O_3

Figure 11: Charles and Hild

Figure 12a: Charles and Hild

Figure 12b: Charles and Hild
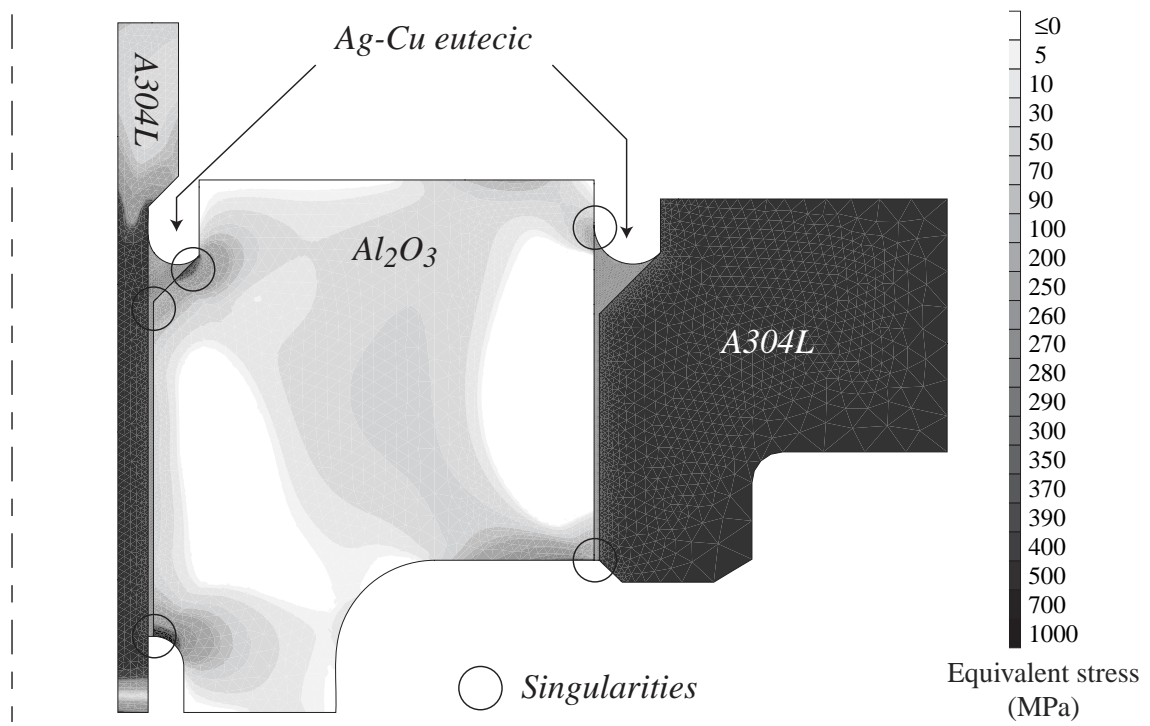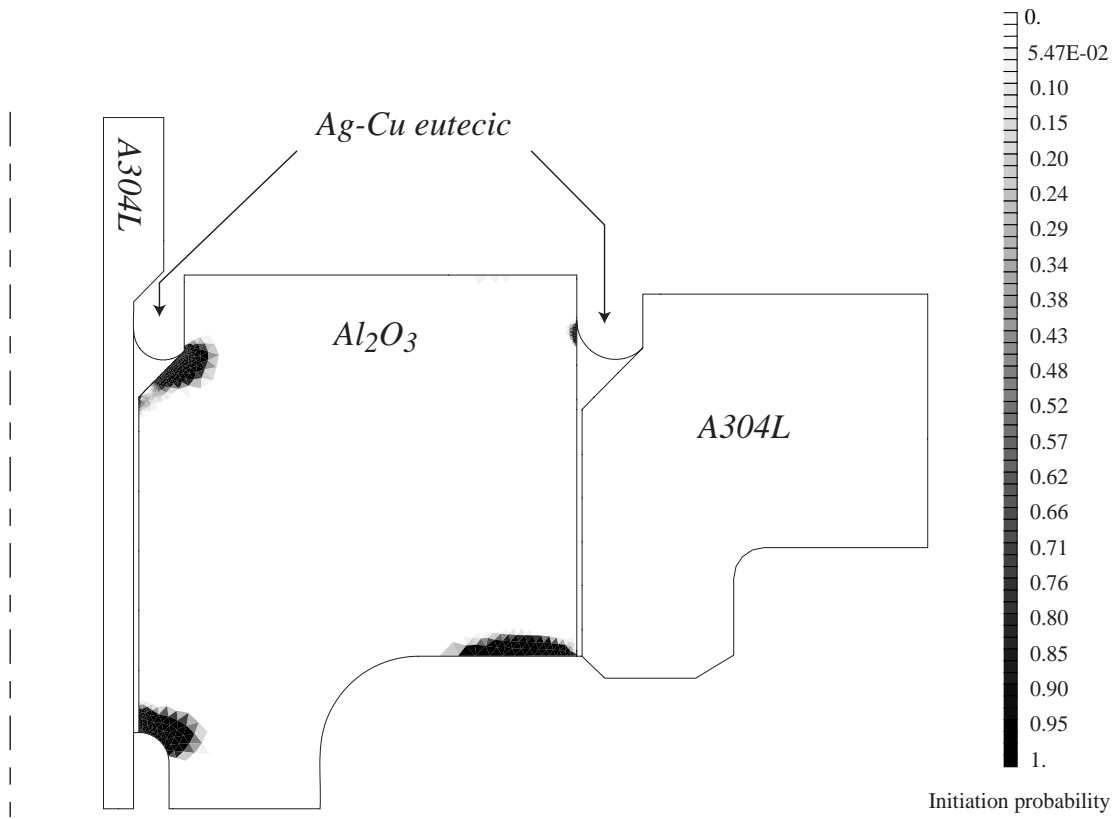
Figure 13: Charles and Hild

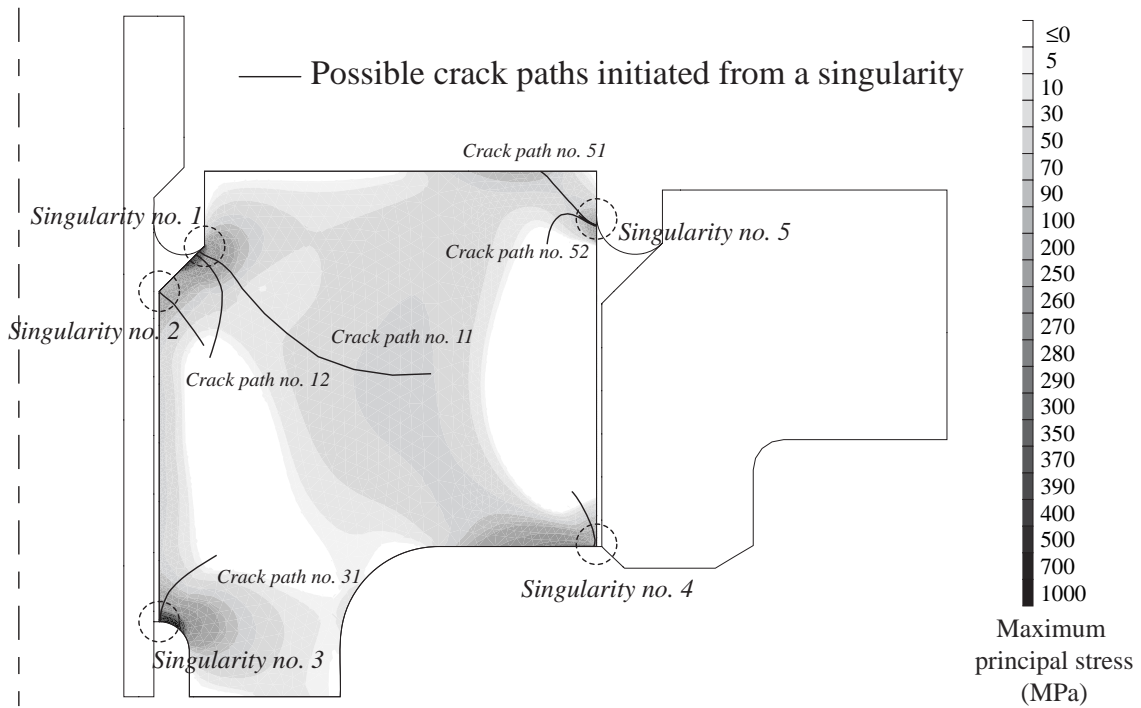**Figure 14: Charles and Hild**

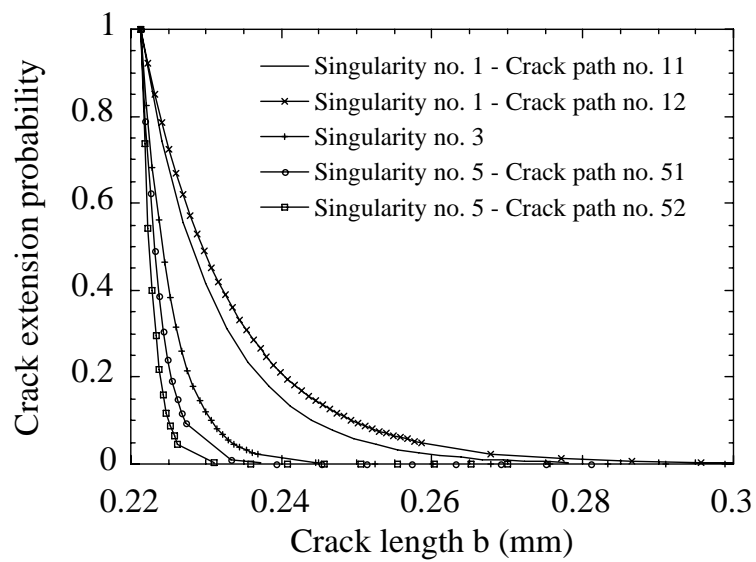**Figure 15a: Charles and Hild**

Figure 15b: Charles and Hild

Table Caption

Table 1: Toughness parameters for a 97% alumina ceramic

Table 2: Indentation parameter $\dfrac{k\lambda^{3/2}}{\Delta K}$ (N^{-1}) for different applied masses (average: 0.45 N^{-1})

Table 3: Singularity exponent at different singularity points

Table 1: Charles and Hild

λ (m^{-1})	α	β	K_c^{max} $(MPa\sqrt{m})$	K_c^{min} $(MPa\sqrt{m})$	M (kg)	$\dfrac{k\lambda^{3/2}}{\Delta K}$ (N^{-1})
5.10^5	2.8	9.1	19.2	0	0.3	0.45

Table 2: Charles and Hild

Mass M (kg)	0.2	0.3	0.5	1
$\dfrac{k\lambda^{3/2}}{\Delta K}$ (N^{-1})	0.52	0.45	0.44	0.45

Table 3: Charles and Hild

Singular point	Singularity exponent at the beginning of the cooling process	Singularity exponent at the end of the cooling process
No. 3	0.41	0.22
No. 5	0.70	0.19